This is a repository copy of *Understanding the influence of SO2 and O2 on the Corrosion of Carbon Steel in Water-Saturated Supercritical CO2*.

Understanding the Influence of SO_2 and O_2 on the Corrosion of Carbon Steel in Water-Saturated Supercritical CO_2

Yong Hua, Richard Barker and Anne Neville
Institute of Functional Surfaces
School of Mechanical Engineering
University of Leeds
Leeds, LS2 9JT
United Kingdom

ABSTRACT

The general and localized corrosion behaviour of carbon steel (UNS G15130) in water-saturated supercritical CO_2 conditions containing O_2 and SO_2 at 35 °C and 8 MPa is evaluated with a view to the effect this may have on pipeline integrity during dense-phase CO_2 transport. The results indicate that crystalline $FeCO_3$ forms in the presence of solely water and CO_2. However, the combined introduction of small concentrations of O_2 and SO_2 (as low as 20 and 2 ppm (mole), respectively) change $FeCO_3$ crystal morphology. Increasing the concentration of SO_2 to 50 and 100 ppm whilst maintaining O_2 content at 20 ppm resulted in the formation of $FeSO_3 \cdot 3H_2O$ as well as $FeCO_3$. In conjunction with the change in corrosion product chemistry and morphology, general corrosion rates of samples increased from 0.1 mm/year to 0.7 mm/year as a result of the rise in SO_2 content from 0 to 100 ppm (based on 48 hour experiments), whilst localized corrosion rates (determined from surface profilometry) rose from 0.9 to 1.7 mm/year. The research demonstrates that localized corrosion measurements are a fundamental requirement when determining the threat posed to carbon steel pipelines during dense-phase CO_2 transport, exceeding the uniform corrosion rate by nearly one order of magnitude under certain conditions. Additional tests involving solution replenishment over 48 hours indicated that the higher corrosion rates observed in the presence of SO_2 did not present the worst case scenario corrosion rates and highlight the importance of having a system where the process fluid is continuously replenished. The corrosion product morphology and chemistry was identified through a combination of scanning electron microscopy (SEM), energy-dispersive X-ray spectroscopy (EDX) and X-ray diffraction (XRD).

Key words: Supercritical CO_2, CO_2 corrosion, carbon steel, carbon capture and storage, sulfur dioxide, oxygen

INTRODUCTION

Regarding the transportation of supercritical carbon dioxide (CO_2) via carbon steel pipelines for the Carbon Capture and Storage (CCS) applications, a range of impurities may exist in the CO_2 stream.[1] The most influential of these impurities in terms of pipeline integrity is considered to be the water content. If the water concentration exceeds the solubility limit, then the break-out of free water can be expected, creating an aqueous phase and leading to potentially excessive corrosion rates.[2]

The segregation of CO_2 in an aqueous phase will lead to the formation of carbonic acid (H_2CO_3) which can lower the pH to ~3.3 at a pressure of 8 MPa.[1] Furthermore, any additional contaminants in the CO_2 stream (such as nitrogen oxides (NO_x), sulfur dionxide (SO_2) and oxygen (O_2) amongst others) will in part also segregate into the aqueous phase, and potentially lower pH further.[1] O_2 is particularly important in influencing corrosion mechanisms as it provides additional cathodic reaction paths for corrosion whilst also inhibiting the formation of protective iron carbonate ($FeCO_3$) which has been shown to form in water-containing supercritical CO_2 environments.[2-4] Furthermore, when SO_2 and O_2 are present together, the formation of sulfurous (H_2SO_3) and/or sulfuric (H_2SO_4) acid is permitted which can play a key role in not only the corrosion mechanisms, but also in the nature and morphology of any corrosion products formed, which may inhibit or accelerate the corrosion kinetics.

Although the impact of CO_2 corrosion has been explored extensively in the oil and gas industry, the research does not readily translate to supercritical CCS systems. The partial pressure of CO_2 transported in a CCS process is considerably higher (7.3-30 MPa)[2] than those encountered in oil and gas transport (typically up to 2 MPa)[2]. Furthermore, not only does the dominant phase change in the system (i.e. CO_2 is the dominant fluid in CCS as opposed to water/hydrocarbons in oil and gas production), but the presence of impurities increase the corrosion risk and their potential influence should not be overlooked. Consequently, there is a requirement to further the understanding of the influence of impurities such as O_2 and SO_2 on corrosion processes in high pressure systems where supercritical CO_2 is the dominant phase.

This article complements the literature already conducted in this area by systematically quantifying the level of localized attack in comparison to general corrosion rate measurements and reviewing the influence of SO_2 at low concentrations similar to those recommended by DYNAMIS[(1)] project[5] and Alstom[†6] from a health and safety perspective (i.e. <100 ppm SO_2 content). The weight loss method and surface profilometry measurements are implemented to review the extent of uniform and localized corrosion, respectively, in water-saturated supercritical CO_2 at 35°C and 8 MPa for concentrations of 2, 50 and 100 ppm SO_2 in the presence of 20 ppm O_2. The nature and morphology of the corrosion products are identified using a combination of scanning electron microscopy (SEM), energy dispersive X-ray spectroscopy (EDX) and X-ray diffraction (XRD) in order to identify the role low concentrations of SO_2 and O_2 play on the corrosion product film composition and morphology. Finally, the validity of the results and the limitations of the test procedure are considered by performing additional tests involving the replenishment of the process fluid. Such an approach provides an appreciation for the influence of SO_2/O_2 consumption throughout the course of the experiment.

EXPERIMENTAL PROCEDURE

Materials and preparation
Test specimens were machined from carbon steel (UNS G15130) into discs of diameter 25 mm and thickness of 6 mm. The chemical composition of the specimen is provided in Table 3. Surface preparation consisted of wet-grinding the entire sample up to 800 grit silicon carbide abrasive paper, rinsing with distilled water, followed by acetone, high purity ethanol and drying gently with compressed air. specimens were then stored in a desiccator until needed and weighed immediately before the experiment on an electronic balance with an accuracy of 0.01 mg before suspending inside the autoclave. Two samples were placed within the autoclave for each individual test, generating a total surface area of approximately 25 cm^2 exposed to the solution.

[(1)] DYNAMIS, CCS project co-funded by the European Commission under the Sixth Framework Porgramme
[†] Trade name

Table 1: Elemental composition of steel (wt.%)

C	Si	Mn	P	S	Cr	Mo	Ni
0.12	0.18	1.27	0.008	0.002	0.11	0.17	0.07
Cu	**Sn**	**Al**	**B**	**Nb**	**Ti**	**V**	**Fe**
0.12	0.008	0.022	0.0005	0.054	0.001	0.057	Balance

Autoclave testing procedure

Figure 1 provides a schematic representation of the experimental system layout. The entire system consists of a 1 litre capacity autoclave, temperature controller, a technical grade of $CO_2/SO_2/O_2$ mixed cylinder, a liquid CO_2 cylinder, a series of valves for flow control and a waste gas treatment system.
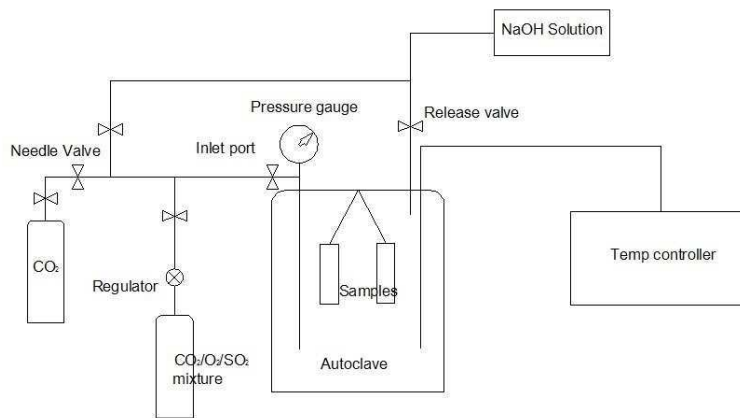

Figure 1: Schematic of autoclave setup

The distilled water used in each experiment was de-aerated by saturating the solution with CO_2 in a separate container for a minimum of 12 hours prior to testing. The specimens were suspended within the autoclave on a non-conducting wire whilst also ensuring they were not in contact with the walls of the cylinder to prevent galvanic effects. The prepared, CO_2-saturated water was carefully delivered into the bottom of the autoclave at ambient pressure and temperature and sealed. All lines to the autoclave were purged with CO_2 and evacuated to ensure the removal of initial traces of O_2 within the system. The required technical grade of $CO_2/SO_2/O_2$ mixture and liquid CO_2 was then transferred into the autoclave, heated and pressurized to the correct temperature and pressure. The starting point of the test is taken from the time at which the autoclave reached the required temperature and pressure. At the end of each experiment, the exhaust gas was filtered through sodium hydroxide (NaOH) solution to prevent release of the residual waste gas into the environment.

All tests were conducted in static conditions in water-saturated supercritical CO_2. According to Spycher et. al.,[7] the saturated water concentration in supercritical CO_2 at 35 °C and 8 MPa is 3437 ppm. In order to ensure the water-saturated CO_2 condition, 34000 ppm of water was introduced to the autoclave for the water-saturated tests (i.e. approximately 10 times the saturation limit). Table 2 provides information on the matrix of tests conducted in this paper.

Table 2: Test matrix for corrosion experiments

Temp. (°C)	Pressure (MPa)	H$_2$O (ppm (mole))	SO$_2$ (ppm (mole))	O$_2$ (ppm (mole))	Immersion time (hours)	Surface analysis techniques
35	8	Water-saturated (3437 ppm in CO$_2$ phase through addition of 34000 ppm water)	0	0	48	X-ray diffraction, scanning electron microscopy, energy dispersive x-ray spectroscopy, surface profilometry measurement
			2	20		
			50	20		
			100	20		

At the end of each test, the specimens were dried thoroughly and photographed. The specimens were subsequently chemically cleaned to remove all traces of corrosion products before weighing. The cleaning process consisted of wiping the surface with a cotton pad soaked in Clarke's solution (20 g antimony trioxide + 50 g stannous chloride + 1000 ml hydrochloric acid) in accordance with ASTM[(2)] Standard G1-03.[8] This was followed by rinsing the specimens with distilled water, followed by drying with compressed air.

The mass loss due to corrosion was determined from the weight difference before exposure and after cleaning. The corrosion rates were calculated by using Equation (1):

$$V_c = \frac{87600 \, \Delta m}{\rho \, A \, t} \qquad (1)$$

where V_c is the corrosion rate of the specimen in mm/year, Δm is the weight loss in grams, ρ is the density of the steel in g/cm^3, A is the exposed area in cm^2 and t is the immersion time in hours.

RESULTS AND DISCUSSION

Mass loss in water-saturated CO$_2$ phase with varying concentrations of SO$_2$ and O$_2$
Mass loss results, which were subsequently averaged to produce a mm/year loss rate over a period of 48 hours, are provided in Figure 2 for carbon steel samples exposed to water-saturated supercritical CO$_2$ at 8 MPa and 35 °C containing different concentrations of SO$_2$ (0, 2, 50 and 100 ppm) and O$_2$ (0 and 20 ppm). After 48 hours of exposure to the water-saturated environment without SO$_2$ and O$_2$, the general corrosion rate averaged 0.10 mm/year. The addition of 2 ppm SO$_2$ and 20 ppm O$_2$ in the gas phase increases the corrosion rate to 0.12 mm/year. As the SO$_2$ content is raised to 50 ppm and 100 ppm (whilst maintaining O$_2$ content), the general corrosion rate in the system increases further to 0.37

and 0.71 mm/year, indicating that SO_2 content can have a profound effect on the corrosion kinetics, even at low concentrations of 100 ppm.

In comparison to the tests performed here, Xiang et. al.,[9] investigated the corrosion behavior of carbon steel in water-saturated supercritical CO_2 environments with the addition of 0.2, 0.7 and 1.4 % of SO_2 and 1000 ppm of O_2 at 10 MPa and 50 °C for 288 hours (Note: 1 % ≈ 10000 ppm). They obtained general corrosion rates of between 0.2 mm/year and 0.9 mm/year which are similar to those recorded in this study, despite the SO_2 content used by Xiang et. al.,[9] being considerably greater. A suggested reason for the discrepancy between these results is that tests performed in this publication are conducted in static conditions whilst Xiang et. al.,[9] performed their experiments in a rotating autoclave at 120 rpm. It is suggested that the presence of flow within the system reduces the amount of water condensed onto the steel surface and subsequently minimizes the level of corrosion throught entrainment of water into the process fluid. Consequently, the results presented here provide a worst case scenario in terms of corrosion rates.

In terms of supporting the theory of the presence of process fluid surface velocities potentially producing lower corrosion rates, the work of Farelas et. al.,[10] demonstrated that the presence of flow (1000 rpm sample rotation speed) reduced corrosion rates of specimens by around an order of magnitude in specific dense phase CO_2 environments. Farelas et. al.,[10] performed tests at 8 MPa in both liquid (25°C) and supercritical (50°C) conditions with the addition of 650 ppm water and 0.08 MPa (0.1 %) SO_2. General corrosion rates reduced as a result of the transition from static to dynamic from 0.03 to 0.02 mm/year in supercritical conditions and from 0.1 to 0.01 mm/year in liquid CO_2.

To add further credence to this argument, Choi et. al.,[2] recorded a corrosion rate of 5.5 mm/year for carbon steel exposed to water-saturated CO_2 containing 1 % SO_2 at 50 °C and 8 MPa, which are very similar to the aforementioned conditions considered by Xiang et. al.,[9] who recorded corrosion rates less than 0.9 mm/year. The two main discrepancies between the two tests were the test duration (24 hours[2] and 288 hours[9], respectively) and the presence of flow (static for Choi et al.,[2] and 120 rpm for Xiang et al.,[9]). Such observations suggest either the presence of flow can significantly reduce corrosion rate, or that initial corrosion rates in the system are very high and begin to decline significantly throughout the test duration due to the development of a protective corrosion product. It is therefore possible that the presence of flow is capable of reducing the level of water accumulation on the steel surface, thereby reducing the corrosion rate in the system compared to that of stagnant conditions. However, such an observation requires further verification.

Corrosion product morphology and composition
Figure 3 provides the SEM images and EDX spectra of the sample surfaces exposed to water-saturated supercritical CO_2 environments containing different levels of SO_2 and O_2 after 48 hours. In each instance the steel surface was found to be locally covered by corrosion products. Figure 4 shows the XRD patterns acquired from each sample surface.

When neither SO_2 nor O_2 were present in the system, the surface of the steel possessed two distinct regions. Region A (Figure 3(a)) consisted of numerous, large, cubic crystals whilst Region B (Figure 3(b)) contained much thinner patches of corrosion product, which upon further inspection consisted of smaller, platelet type crystals. The difference in crystal morphology is believed to be related to the quantity of water which condensed and accumulated at the surface of each sample, which has been shown to give rise to different nucleation and growth behavior of $FeCO_3$.[12] (In Region A, a larger amount of water has condensed onto the steel surface relative to Region B. The EDX spectra present in Figures 3(a) and (b) show that both crystals contain oxygen, carbon, iron and the XRD pattern in Figure 4 confirms the presence of $FeCO_3$ crystals on the steel surface.
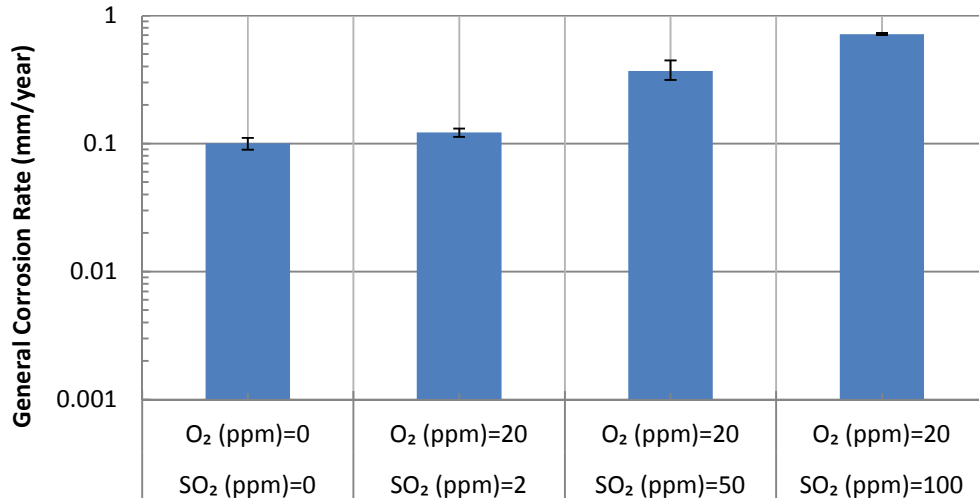
Figure 2: General corrosion rates of carbon steel in the water-saturated CO$_2$ phase at 8 MPa and 35 °C for an exposure time of 48 hours, containing SO$_2$ (0, 2, 50 and 100 ppm) and O$_2$ (0 and 20 ppm)

Figures 3(c) and (d) indicate that the introduction of 2 ppm SO$_2$ and 20 ppm O$_2$ resulted in a change in the morphology of the crystalline deposit, producing globular sets of fine crystals which were confirmed as FeCO$_3$ through the XRD pattern also provided in Figure 4. It is worth noting that no other crystalline deposits were detected within the corrosion film using XRD. Interestingly however, strong traces of sulfur were detected on the steel surface through EDX measurements shown in Figures 3(c) and (d). This perhaps suggests that any sulfur compounds present on the surface are amorphous in nature, or that the corrosion products are so thin that they eluded detection by XRD.

The increase in SO$_2$ to 50 ppm produced samples which were visibly more corroded than tests performed at the lower SO$_2$ concentration. The sample surfaces in Figures 3(e) and (f) bear a striking resemblance to those observed by Choi et al.,[2] in tests performed in water-saturated CO$_2$ at 8 MPa and 50 °C with 0.08 MPa SO$_2$. Choi et al.,[2] detected the presence of hydrated iron sulfite (FeSO$_3$·3H$_2$O) on the steel surface and found no indication of the presence of FeCO$_3$ according to Raman spectroscopy. However, the lower content of SO$_2$ used in the experiments within this publication has resulted in the co-presence of both FeCO$_3$ and FeSO$_3$·3H$_2$O as shown in Figure 4. Many regions of the surface consisted of columnar crystals with quite a regular structure (Figure 3(e)), whilst other regions of the surface produced a flat, cracked film with a high sulfur content, which could potentially provide channels for further corrosion reactions (Figure 3(d)).

Final tests performed with the addition of 100 ppm SO$_2$ and 20 ppm O$_2$ again produced two distinct areas of corrosion. Region A (Figure 3(g)) showed the presence of columnar iron sulfite crystals, whilst Region B (Figure 3(h)) showed signs of cellular shaped crystals which also possessed a high sulfur content. Referring to the XRD pattern in Figure 4 and from detailed SEM analysis, it became evident that as SO$_2$ content in the system increased, the relative ratio between FeSO$_3$ and FeCO$_3$ on the steel surface became much greater. Literature also suggests that increasing the SO$_2$ content to even higher concentration such as 0.2 mol.% completely supresss the formation of any FeCO$_3$ on the steel surface.[9]

These observations indicate that the combined presence of very small quantities of SO$_2$/O$_2$ have the ability to strongly influence the corrosion behavior in the system. The results demonstrate that SO$_2$ has the ability to take the leading role in the corrosion process despite its low relative concentration when compared to CO$_2$ in the system.
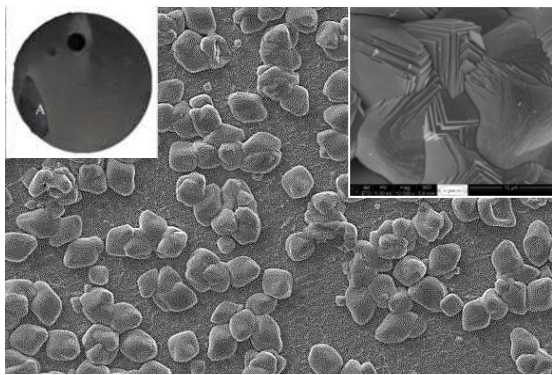
Mag = 1.00 KX   20.00 kV   SE1   10 μm
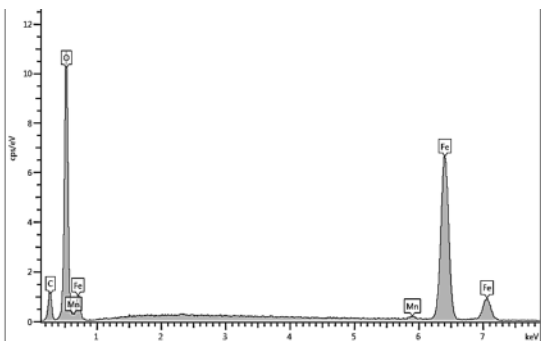
(a)
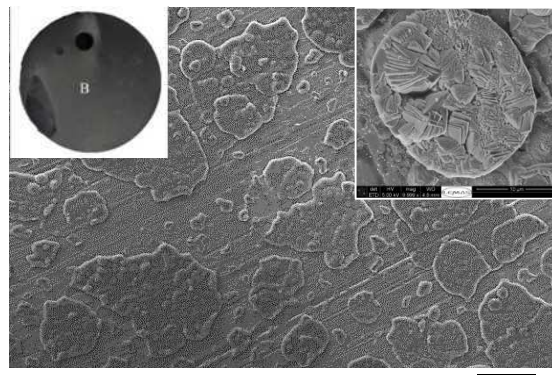
Mag = 1.00 KX   20.00 kV   SE1   10 μm

(b)
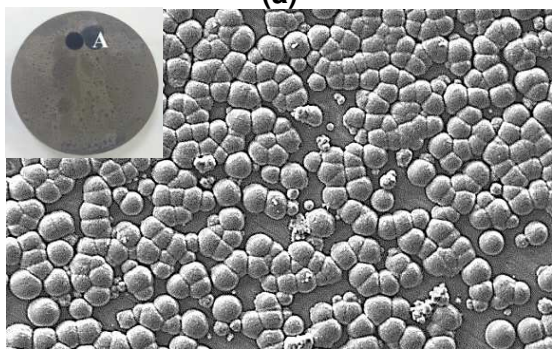
Mag = 1.00 KX   20.00 kV   SE1   10 μm
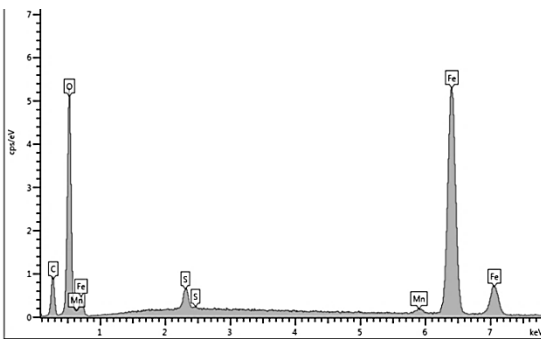
(c)
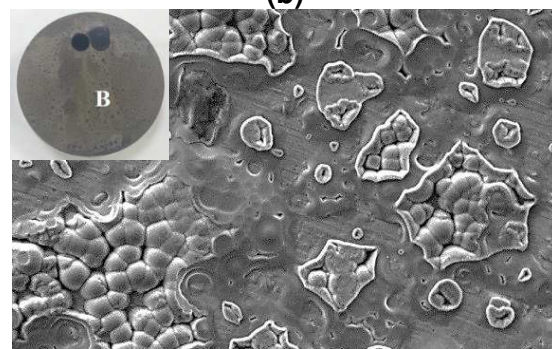
Mag = 1.00 KX   20.00 kV   SE1   10 μm
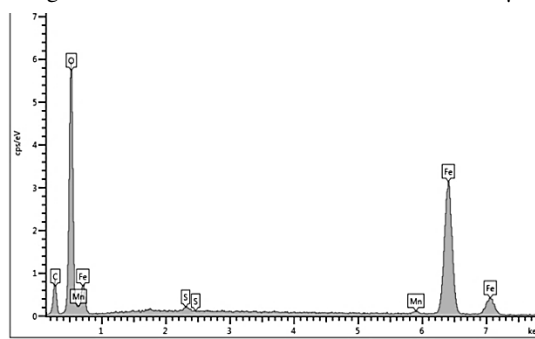
(d)
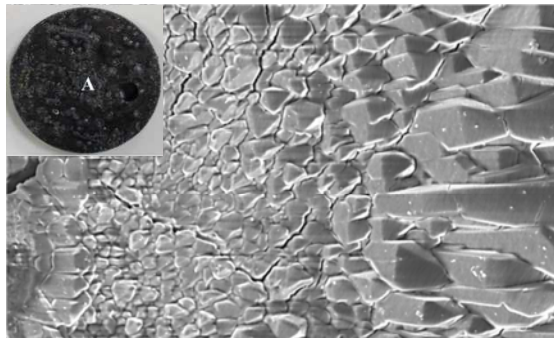
Mag = 1.00 KX   20.00 kV   SE1   10 µm
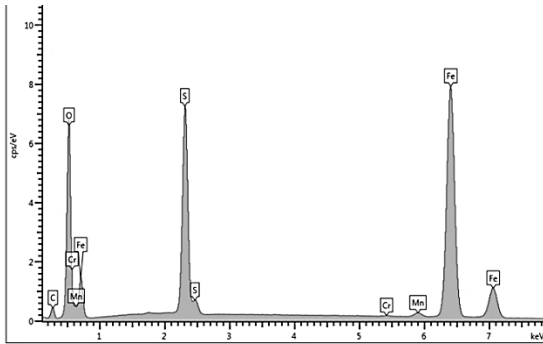
(e)
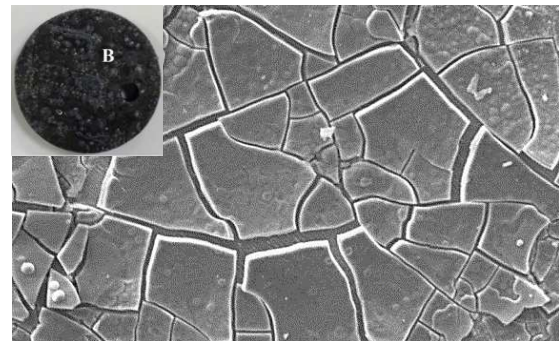
Mag = 1.00 KX   20.00 kV   SE1   10 µm
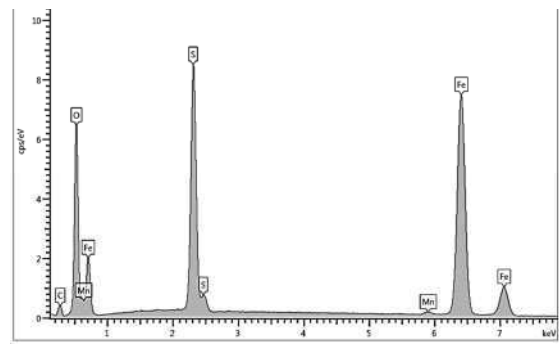
(f)
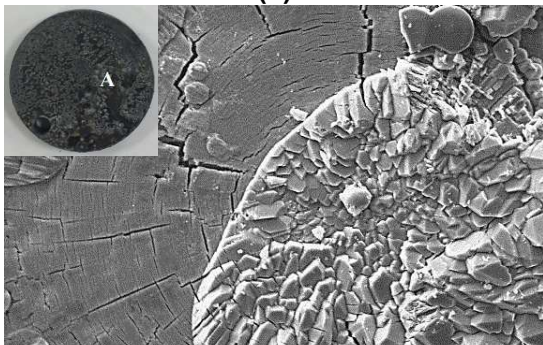
Mag = 1.00 KX   20.00 kV   SE1   10 µm
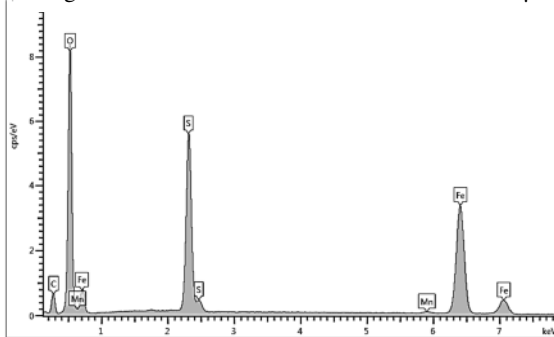
(g)
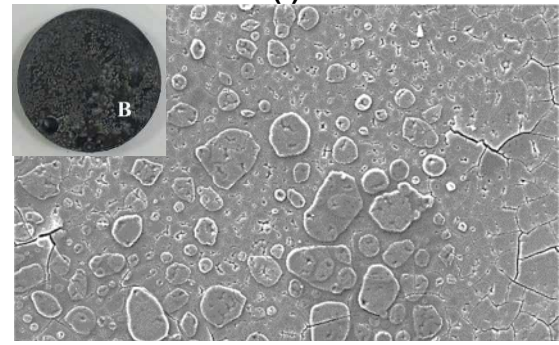
Mag = 1.00 KX   20.00 kV   SE1   10 µm
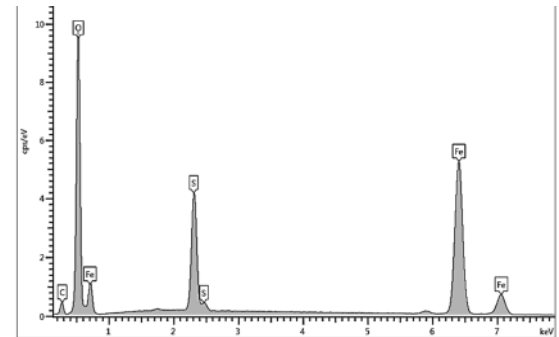
(h)

Figure 3: SEM images of the corroded samples exposed to water-saturated CO_2 at 35 °C and 8 MPa for 48 hours (a) 0 ppm SO_2 and 0 ppm O_2 – Region A (b) 0 ppm SO_2 and 0 ppm O_2 – Region B (c) 2 ppm SO_2 and 20 ppm O_2 – Region A (d) 2 ppm SO_2 and 20 ppm O_2– Region B (e) 50 ppm SO_2 and 20 ppm O_2 – Region A (f) 50 ppm SO_2 and 20 ppm O_2 – Region B (g) 100 ppm SO_2 and 20 ppm O_2 – Region A (h) 100 ppm SO_2 and 20 ppm O_2 – Region B
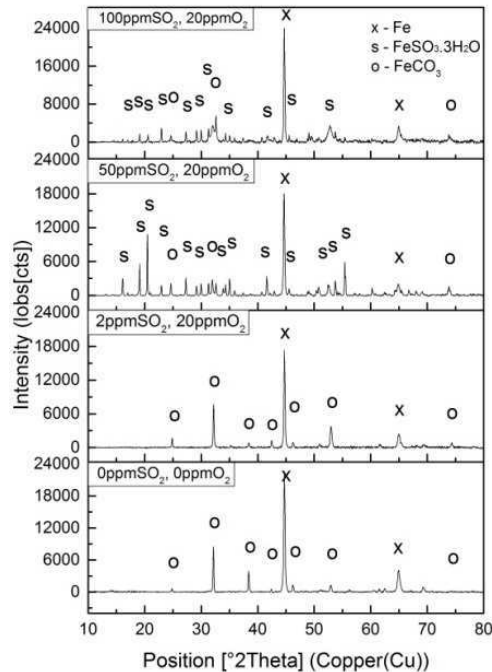
**Figure 4: XRD pattern of samples surfaces after exposure to water-saturated supercritical CO_2 phase at 35 °C and 8 MPa conataing different concentration levels of SO_2 and O_2**

Surface pitting analysis

Figure 5 provides examples of the profilometry measurements extracted from the samples exposed to the water-saturated CO_2 environment at 35 °C and 8 MPa with various concentrations of SO_2 and O_2 present in the system. The profilometry images are provided in conjunction with the general corrosion rates (from mass loss measurements) and the localized corrosion rates based on the top 10 deepest surface pits identified in alignment with ASTM[(3)] Standard G46-94.[11]

Figure 5 indicates that the localized corrosion rates (when considering the entire corroded surface) are approximately one order of magnitude greater (in some instances) than the general corrosion rates calculated through the implementation of mass loss measurements. The localized corrosion rate increases from 0.9 mm/year to 1.7 mm/year from the system containing no SO_2/O_2 to that containing 100 ppm SO_2 and 20 ppm O_2. These results, to a certain extent, are in alignment with the observation of Farelas et. al.,[12] who performed experiments in liquid CO_2 at 25 °C and 8 MPa in under-saturated containing 650 ppm water and identified that localized corrosion rates are significant in such systems. Mass loss measurements after 24 hours of exposure revealed general corrosion rates of 0 and 0.1 mm/year in the presence of 0.05 and 0.1% SO_2, respectively. However, implementation of infinite focus microscopy indicated localized corrosion rates of 2.4 and 6.8 mm/year, respectively. Both the work presented in this publication and the results of Farelas et. al.,[12] indicate that mass loss results can be misrepresentative in terms of the threat posed to carbon steel exposed to impurity containing dense phase CO_2.

Further analysis of the surface pits indicated that increasing the SO_2 content in the system resulted in an increase in depth, but also promoted a change in their shape. As SO_2 concentration increased, the pits, or regions of localized attack became wider as well as deeper, making the regions of attack much more significant. The differences in pitting morphology can be observed in Figure 5 when considering the 2D surface profiles of the samples exposed to the systems containing both 2 and 100 ppm SO_2.

[(3)] ASTM International, 100 Barr Harbor Drive, West Conshohocken, PA 19428-2959.

Replenishment of impurities and the limitations of closed system testing

Regrettably, one of the issues associated with experiments in closed systems with low impurity concentrations is that significant levels of depletion can occur in the system over the course of the experiment. Dugstad et. al.,[13] stated that less that 5% of the added impurities required consumption in NO_X and SO_X experiments before the corrosion rate slows down. They also stated that the difference in impurity concentration at start up and when the experiment is terminated is considerably larger than that estimated from purely the mass loss of the steel samples. Such an observation was attributed to a multitude of factors which include immobilization of the impurities (corrosive phase becoming trapped in dead legs) as well as reactions between different impurities in the system.[13]

Based on the observations of Dugstad et. al.,[13] it can be questioned as to whether the corrosion rates in this paper reflect the worst case scenario in terms of the level of attack. To investigate this effect of depletion, a series of tests performed in the previous section were extended to 96 hours. A selection of these tests were left for 96 hours, whilst in other tests the solution was evacuated and replenished after 48 hours, enabling the effect of replenishing impurities on the corrosion rate to be observed.

Table 4 indicates the tests performed in this additional section. Again, an assessment of the corrosion products (using XRD) and the general and localized pitting behavior (using mass loss and profilometry, respectively) was performed.

Table 4: Test matrix to investigate the effects of solution replenishment

Temp. (℃)	Pressure (MPa)	H_2O (ppm mole)	SO_2 (ppm mole)	O_2 (ppm mole)	Immersion time (hours) Total	Immersion time (hours) Replenish Fluid	Surface Analysis Techniques
35	8	Water-saturated (3437 ppm in CO_2 phase through addition of 34000 ppm water)	50	20	96	Not replenished	X-ray diffraction, scanning electron microscopy, surface profilometry measurement.
						Replenished after 48 hours	
			100			Not replenished	
						Replenished after 48 hours	

Mass loss results are provided in Figure 6 for carbon steel samples exposed to water-saturated supercritical CO_2 at 8 MPa and 35 ℃ with and without replenishing impurities. It is clear that replenishing the process fluid results in a greater corrosion rate. For the system containing 50 ppm SO_2 and 20 ppm O_2, corrosion rate increased from 0.27 to 0.39 mm/year as a result of replenishing the solution, whilst the corrosion rate in the system containing 100 ppm SO_2 and 20 ppm O_2 increased by 30% from 0.50 to 0.65 mm/year.
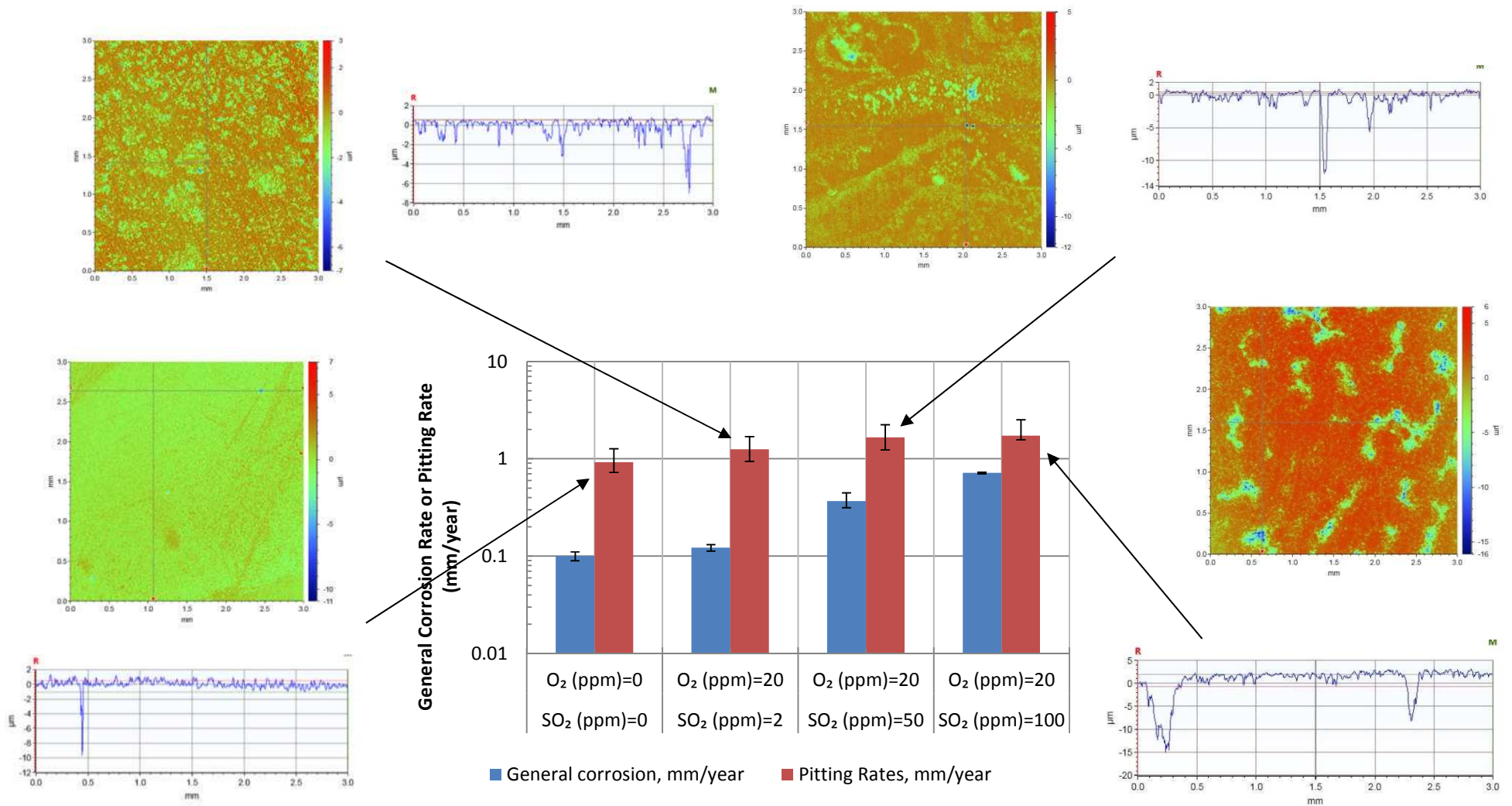
Figure 5: Average general corrosion and pitting rates of carbon steel in water-saturated supercritical CO_2 environments containing varying concentrations of SO_2 and O_2 at 35 °C and 8 MPa for 48 hours, presented in conjunction with profilometry images of the samples
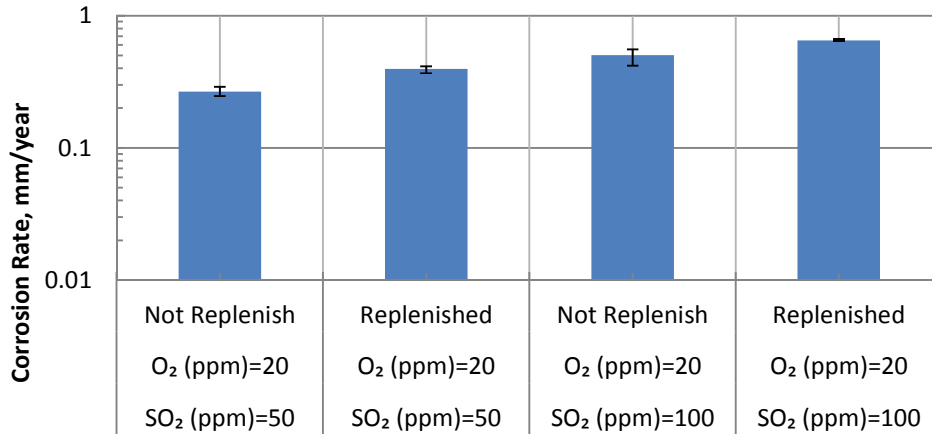
Figure 6: General corrosion rates of carbon steel in the water-saturated CO$_2$ phase at 8 MPa and 35 ℃ for an exposure time of 96 hours, containing SO$_2$ (50 and 100 ppm) and O$_2$ (0 and 20 ppm), with and without impurity replenishment

Figure 7 provides the SEM images of the samples surface exposed to water-saturated supercritical CO$_2$ environments with and without replenishing the solution over 96 hours. Although difficult to tell from discrete SEM images, general observations of the surfaces indicated that there was very little difference in the morphology of the corrosion products on the steel surfaces, despite there being a number of different crystal structures observed on the steel surface.

| Mag = 144 X | 20.00 kV | SE1 | 200 µm | Mag = 1.00 KX | 20.00 kV | SE1 | 10 µm |

(a)

| Mag = 144 X | 20.00 kV | SE1 | 200 µm | Mag = 1.00 KX | 20.00 kV | SE1 | 10 µm |

(b)
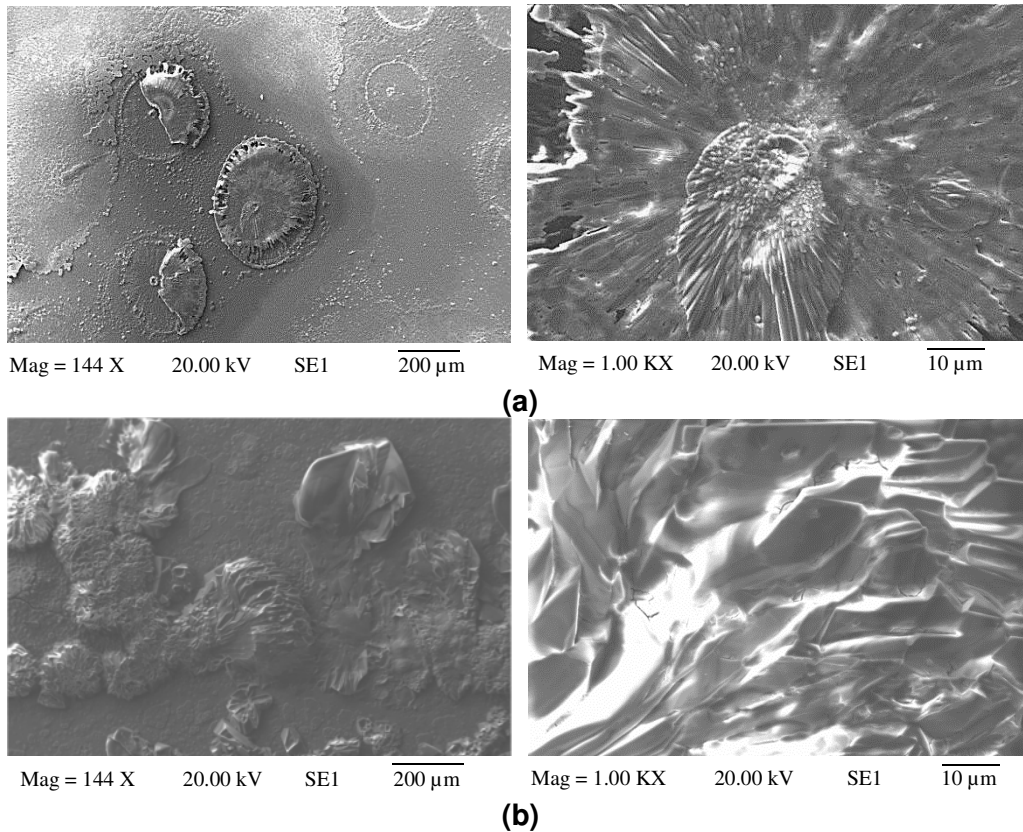
Figure 7: SEM images of the corroded samples exposed to water-saturated CO$_2$ at 35 ℃ and 8 MPa containing 50 ppm SO$_2$ and 20 ppm O$_2$ for 96 hours (a) without and (b) with replenishing the test solution after 48 hours

In terms of the XRD analysis of the samples, an increase in relative intensity between $FeSO_3$ and $FeCO_3$ was observed as a result of replenishing the test solution. The increase in relative intensity indicates a higher quantity of $FeSO_3$ on the surface relative to $FeCO_3$. A much greater intensity for $FeSO_3$ was observed from the sample exposed to the replenished solution, suggesting a greater quantity of corrosion product on the steel surface, which coincides to a certain extent with the increase in corrosion rate which would essentially supply more Fe^{2+} ions in to the aqueous solution for precipitation of corrosion products to occur.
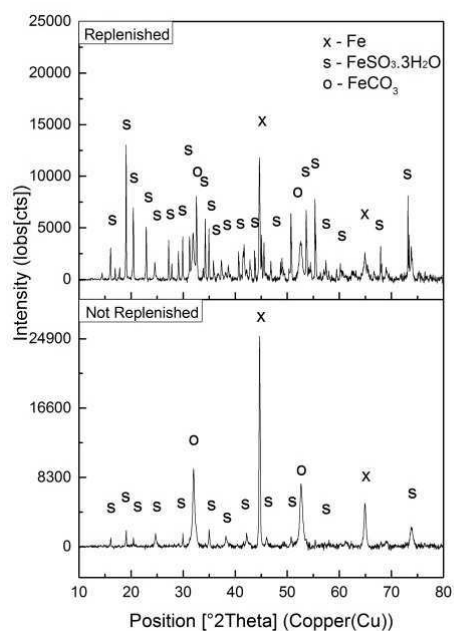

Figure 8: XRD patterns of samples surfaces after exposure to water-saturated supercritical CO_2 phase at 35 °C and 8 MPa for 96 hours with and without replenishing 50 ppm of SO_2 and 20 ppm of O_2 after 48 hours

Figure 9 provides examples of the profilometry measurements taken from the samples exposed to the water-saturated CO_2 environment at 35 °C and 80 MPa containing various concentrations of SO_2 and O_2 with and without solution replenishment over 96 hours. The profilometry images are provided in conjunction with the general corrosion rates (from mass loss measurements) and the localized corrosion rates based on the top 10 deepest surface pits identified (from surface profilometry).

Figure 9 indicates that the localized corrosion rates in the presence of 50 ppm SO_2 and 20 ppm over 96 hours increase on average as a result of replenishing the test fluid. Changing the solution after 48 hours resulted in average pitting rates of 1.3 mm/year in contrast to 1.0 mm/year. Similar observations occurred in the system containing 100 ppm SO_2 and 20 ppm O_2 where an increase from 1.1 to 1.5 mm/year was recorded through changing the solution. However, it is important to note that although the maximum and average pit depths as a result of solution replenishment did increase, the error bars in pit depths across the top 10 deepest pits do overlap, indicating this may not be a significant difference in pitting rate. What is evident, is the significant difference in general corrosion rate between the two systems which clearly demonstrate the limitations of implementing a closed system to obtain reliable quantitative corrosion rate data relating to the transport of impurity-containing supercritical CO_2.
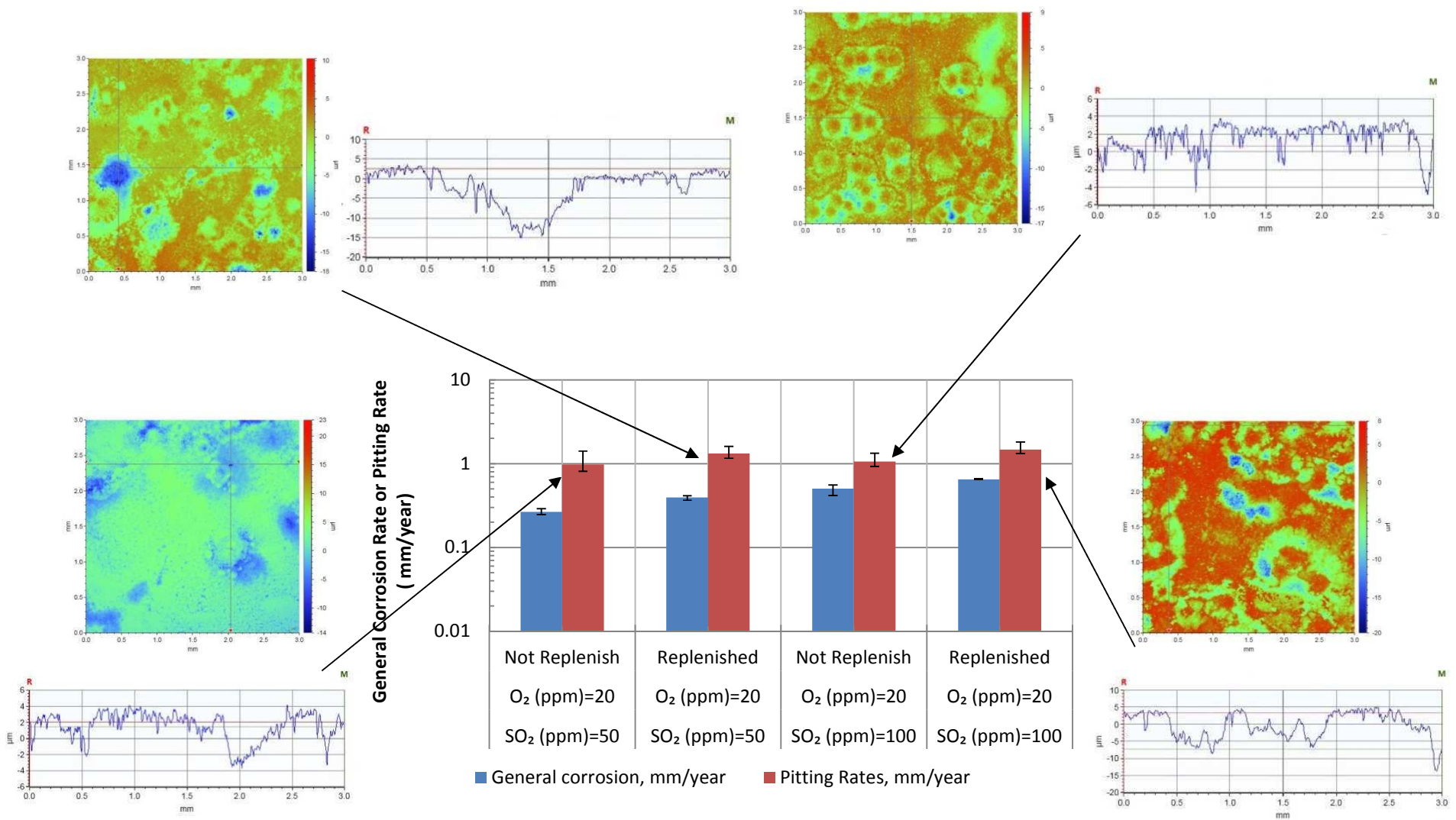
Figure 9: Average general corrosion and pitting rates of carbon steel in water-saturated supercritical CO$_2$ environments mixed with varying concentrations of SO$_2$ and O$_2$ at 35 °C and 8 MPa for 96 hours, presented in conjunction with profilometry images of the samples – tests are with and without solution replenishment after 48 hours

Discussion of reaction mechanisms

Both $FeCO_3$ and $FeSO_3 \cdot 3H_2O$ were identified on the surface of the carbon steel samples exposed to the environments containing between 2 and 100 ppm SO_2, whilst only $FeCO_3$ was detected on the surface without the presence of SO_2.

As discussed by Cole et. al.,[14] in terms of the formation of $FeCO_3$, three series of reactions are capable of occurring within steel pipelines which transport supercritical CO_2 when water condenses onto the steel surface. These reactions are:

a) The saturation of the condensed water with CO_2, its association to produce carbonic acid and its subsequent partial homogenous dissociation in two steps to form bicarbonate and carbonate ions:

$$CO_{2(g)} \leftrightarrow CO_{2(aq)} \tag{2}$$

$$CO_{2(g)} + H_2O_{(l)} \leftrightarrow H_2CO_{3(aq)} \tag{3}$$

$$H_2CO_3 \leftrightarrow H^+ + HCO_3^- \tag{4}$$

$$HCO_3^- \leftrightarrow H^+ + CO_3^{2-} \tag{5}$$

b) In the next stage of reactions, the cathodic reaction can occur either by direct reduction of hydrogen ions, or the reduction of carbonic acid or carbonate ions:

$$2H^+ + 2e^- \leftrightarrow H_2 \tag{6}$$

$$2H_2CO_3 + 2e^- \rightarrow H_2 + 2HCO_3^- \tag{7}$$

$$2\,HCO_3^- + 2\,e^- \rightarrow H_2 + 2\,CO_3^{2-} \tag{8}$$

c) The final stage is the anodic dissolution of iron:

$$Fe \rightarrow Fe^{2+} + 2e^- \tag{9}$$

Which can be followed by the precipitation of $FeCO_3$ via a one stage reaction with carbonates, or via a two stage reaction with bicarbonates:

$$Fe^{2+} + CO_3^{2-} \rightarrow FeCO_3 \tag{10}$$

$$Fe^{2+} + 2HCO_3^- \rightarrow Fe(HCO_3)_2 \tag{11}$$

$$Fe(HCO_3)_2 \rightarrow FeCO_3 + CO_2 + H_2O \tag{12}$$

As can be observed from the XRD analysis of the steel samples, SO_2 is capable of playing a key role in the corrosion mechanisms. The formation of $FeSO_3$ can be described by the following reactions:

a) Firstly, SO_2 is believed to dissolve into the condense water film on the surface and subsequently becomes ionized:

$$H_2O + SO_2 \rightarrow H^+ + HSO_3^{2-} \tag{13}$$

$$\mathrm{HSO_3^{2-} \rightarrow H^+ + SO_3^{2-}} \tag{14}$$
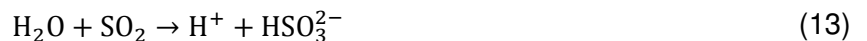
b) The cathodic reaction then occurs via the direct reduction of hydrogen ions:

$$\mathrm{2\,H^+ + 2\,e^- \leftrightarrow H_2} \tag{15}$$

c) The formation of $FeSO_3$ then occurs via a precipitation process:

$$\mathrm{Fe^{2+} + SO_3^{2-} \rightarrow FeSO_3} \tag{16}$$

$FeSO_3 \cdot 3H_2O$ was observed by both Choi et. al.,[2] and Xiang et. al.,[9] in SO_2-containing dense phase CO_2 experiments. Additionally, both these authors detected the presence of $FeSO_4$ on the steel surface, when O_2 was introduced into the system. Choi et al.,[2] performed tests at 8 MPa and 50 °C in water-saturated CO_2 containing 0.08 MPa SO_2 and 0.33 MPa O_2 whilst Xiang et. al.,[9] conducted tests at 10 MPa and 50 °C in water-saturated CO_2 with the addition of 0.02-0.2 MPa SO_2 and 1000 ppm O_2. In both instances $FeSO_4$ was detected on the steel surface.

It was suggested that the addition of O_2 not only results in an additional cathodic reaction (Equation 17), but it also enables the oxidation of sulphate ions to sulphate ions (Equation 18):

$$\mathrm{O_2 + 4H^+ + 4e^- \rightarrow H_2O} \tag{17}$$

$$\mathrm{2\,SO_3^{2-} + O_2 \rightarrow 2\,SO_4^{2-}} \tag{18}$$

$FeSO_4$ then forms via the following reaction:

$$\mathrm{Fe^{2+} + SO_4^{2-} \rightarrow FeSO_4} \tag{19}$$

$FeSO_4$ was the believed by Choi et. al.,[2] to undergo further oxidation to become FeOOH in the presence of O_2 in an acid regeneration process:

$$\mathrm{4\,FeSO_4 + 6\,H_2O + O_2 \rightarrow 4\,FeOOH + 4\,H_2SO_4} \tag{20}$$

It is apparent that the low concentration of 20 ppm O_2 administered in these tests was not sufficient enough to form appreciable amounts (if any) of $FeSO_4$. It has been suggested that $FeSO_3$ and $FeSO_4$ are both hygroscopic salts, capable of enhancing the ability of a sample surface to retain water. Such a process could potentially influence the corrosion rate at the steel surface, particularly if the aforementioned acid regeneration process is capable of occurring.

General discussion
Ultimately, the level of impurities tolerated within dense-phase CO_2 for the purposes of storage and EOR will be dictated by what is economically feasible in terms of removal at capture, what can realistically be transported in conventional pipelines, and the impact of these impurities on the storage reservoirs. This article has focused on the internal corrosion threat posed to pipelines within a $CO_2/H_2O/SO_2/O_2$ system under supercritical conditions.

The results have shown that carbon steel in the presence of water-saturated supercritical CO_2 at 8 MPa and $35^{\circ}C$ produces a low general corrosion rate of 0.1 mm/year in the absence of SO_2 and O_2, although pitting rates were high. However, the introduction of very small quantities of SO_2 and O_2 together have the ability to change the morphology and composition of the corrosion products on the steel surface, as well as accelerating the kinetics of the corrosion reaction. It is important to know that even the presence of 2 ppm SO_2 and 20 ppm O_2 was capable of increasing corrosion rates and influencing the corrosion product morphology.

The results demonstrate some of the complexities associated with understanding and accurately quantifying the corrosion behavior of carbon steels and the threat to pipeline integrity during impure dense-phase CO_2 transport. One of the main issues is the consumption of impurities within the system which prevent long duration tests from being performed. There is therefore a requirement for the impurities to be replenished periodically if long term testing is necessary, or for the use of a once-through system to prevent consumption altogether. In terms of the selection of impurity concentrations within this publication, the upper values chosen from a health and safety perspective.[5, 6] These results are important as the impurity contents are lower and could be agreed as being more representative of what may be encountered during dense-phase CO_2 transport.

Another important observation from this work is that the degradation in all experiments was highly localized. Not only was the combination of SO_2 and O_2 shown to influence pitting severity, but the pitting rates recorded were nearly one order of magnitude greater than the uniform corrosion rate determined from mass loss measurements in some instances. The increase in SO_2 content was also shown to influence the shape of pits as well as their overall depth. In particular, the work highlights the importance of adopting a systematic approach when determining pitting behavior of carbon steels exposed to impure dense-phase CO_2.

Finally, one of the points outlined in this research is whether the corrosion products have the ability to offer protection to the steel substrate. It is well known in the oil and gas industry that $FeCO_3$ is capable of blocking active sites on the steel surface and acting as a diffusion barrier to electrochemically active species involved in the charge-transfer reaction. The ability of $FeSO_3$ to offer similar protection to the steel surface was suggested by Xiang et al.,[15] from their work. However, because of the gradual consumption of SO_2 and O_2 throughout their 192 hour experiment, it is difficult to ascertain whether the reduction in corrosion rate was attributed to solely protective film formation.

Interestingly, comparing the general corrosion rates provided in Figure 2 (50 and 100 ppm SO_2 over 48 hours) and Figure 6 (replenished tests for 50 and 100 ppm SO_2 over 96 hours), there is no observed reduction in the corrosion rate of samples. These results strongly suggest that the $FeSO_3/FeCO_3$ corrosion products formed in this instance resulted in no significant reduction in corrosion rate. It is worth noting that longer duration tests were performed by Xiang et al.,[15], which may have enabled a thicker, more substantial, and potentially protective corrosion product to be developed. Regardless, the topic of corrosion of pipelines still represents a largely overlooked research area which requires further attention, particularly in the role of impurities on corrosion product formation and morphology, and how this links to the corrosion kinetics on both a general and localized scale.

CONCLUSIONS

The research presented has focused towards understanding the extent of both general and localized corrosion of carbon steel in water-saturated supercritical CO_2 environments containing various concentrations of SO_2 (0-100 ppm) and O_2 (0-20 ppm), representative of dense-phase CO_2 transport. Tests were conducted at a pressure of 8 MPa and a temperature of $35^{\circ}C$ for 48 hours and 96 hours

(with and without replenishment of the test fluid). The main conclusions which can be drawn from this study are:

- In the water-saturated supercritical CO_2 environment, the average general corrosion rates for samples over 48 hours were recorded at between 0.12 mm/year and 0.71 mm/year when the SO_2 concentration increased from 2 ppm to 100 ppm in the presence of 20 ppm O_2. General corrosion rate without SO_2 and O_2 was recorded at 0.1 mm/year.

- The results indicate that even small quantities of SO_2 are capable of influencing the degradation process and increasing corrosion kinetics in a water-saturated environment.

- Addition of 2-100 ppm SO_2 with 20 ppm O_2 resulted in the presence of $FeSO_3.3H_2O$ on the steel surface in conjunction with $FeCO_3$. As SO_2 concentration increased, the ratio of $FeSO_3$ to $FeCO_3$ also increased. The quantity of O_2 (fixed at 20 ppm) in the system was not substantial enough to result in any detectable formation of $FeSO_4$.

- The general corrosion rate on the steel surface was nearly one order of magnitude smaller than the rate of surface pitting/localized attack and was shown to be a fundamental consideration in determing the threat to dense phase CO_2 transport pipelines. The extent of localized attack was observed to become more severe with increasing SO_2 content.

- Additional tests involving the replenishment of the process fluid indicated that the general and localized corrosion rates in the closed system tests may not reflect a worst scenario of the damage caused to CO_2 transportation pipelines, and that the resulting scale formation on the steel surface offered very little protection with regards to general corrosion.

REFERENCES

1. I.S. Cole, D.A. Paterson, P. Corrigan, S. Sim, and N. Birbilis, "State of the aqueous phase in liquid and supercritical CO_2 as relevant to CCS pipelines", International Journal of Greenhouse Gas Control, 7, 0 (2012): p. 82-88.
2. Y.-S. Choi, S. Nesic, and D. Young, "Effect of impurities on the corrosion behavior of CO_2 transmission pipeline steel in supercritical CO_2−water environments", Environmental Science & Technology, 44, 23 (2010): p. 9233-9238.
3. Y.-S. Choi and S. Nešić, "Determining the corrosive potential of CO_2 transport pipeline in high pCO_2–water environments", International Journal of Greenhouse Gas Control, 5, 4 (2011): p. 788-797.
4. Y. Hua, R. Barker, and A. Neville, "Effect of temperature on the critical water content for general and localised corrosion of X65 carbon steel in the transport of supercritical CO_2", International Journal of Greenhouse Gas Control, 31, (2014): p. 48-60.
5. E. de Visser, C. Hendriks, M. Barrio, M.J. Mølnvik, G. de Koeijer, S. Liljemark, and Y. Le Gallo, "Dynamis CO_2 quality recommendations", International Journal of Greenhouse Gas Control, 2, 4 (2008): p. 478-484.
6. A. Dugstad, B. Morland, and S. Clausen, "Corrosion of transport pipelines for CO_2–Effect of water ingress", Energy Procedia, 4, (2011): p. 3063-3070.
7. N. Spycher, K. Pruess, and J. Ennis-King, "CO_2-H_2O mixtures in the geological sequestration of CO_2. I. Assessment and calculation of mutual solubilities from 12 to 100°C and up to 600 bar", Geochimica et Cosmochimica Acta, 67, 16 (2003): p. 3015-3031.
8. ASTM Standard G1-03, Standard practice for preparing, cleaning, and evaluating corrosion test specimens. ASTM International: West Conshohocken, PA, 2003.

9.   Y. Xiang, Z. Wang, C. Xu, C. Zhou, Z. Li, and W. Ni, "Impact of SO_2 concentration on the corrosion rate of X70 steel and iron in water-saturated supercritical CO_2 mixed with SO_2", The Journal of Supercritical Fluids, 58, 2 (2011): p. 286-294.

10.   F. Farelas, Y.S. Choi, and S. Nesic. "Effects of CO_2 phase change, SO_2 content and flow on the corrosion of CO_2 transmission pipeline steel", CORROSION 2012, paper no. 1322, (Salt Lake City, UT:NACE, 2012).

11.   ASTM Standard G46-94, Standard guide for examination and evaluation of pitting corrosion. ASTM International: West Conshohocken, PA, 2003.

12.   F. Farelas, Y.S. Choi, and S. Nešić, "Corrosion Behavior of API 5L X65 Carbon Steel under Supercritical and Liquid Carbon Dioxide Phases in the Presence of Water and Sulfur Dioxide", Corrosion, 69, 3 (2012): p. 243-250.

13.   A. Dugstad, M. Halseid, and B. Morland, "Effect of SO_2 and NO_2 on corrosion and solid formation in dense phase CO_2 pipelines", Energy Procedia, 37, (2013): p. 2877-2887.

14.   I.S. Cole, P. Corrigan, S. Sim, and N. Birbilis, "Corrosion of pipelines used for CO_2 transport in CCS: Is it a real problem?", International Journal of Greenhouse Gas Control, 5, 4 (2011): p. 749-756.

15.   Y. Xiang, Z. Wang, Z. Li, and W.D. Ni, "Effect of Exposure Time on the Corrosion Rates of X70 Steel in Supercritical $CO_2/SO_2/O_2/H_2O$ Environments", Corrosion, 69, 3 (2012): p. 251-258.